Research in Astronomy and Astrophysics, 24:115014 (10pp), 2024 November https://doi.org/10.1088/1674-4527/ad862a

Bar Presence in Local Galaxies: Dependence on Morphology in Field Galaxies

M. A. Chacón[1], R. Delgado-Serrano[1], and B. Cervantes Sodi[2]
[1] Dirección Nacional de Ciencias Espaciales, Universidad Tecnológica de Panamá, Panamá; manuel.chacon@utp.ac.pa
[2] Instituto de Radioastronomía y Astrofísica, Universidad Nacional Autónoma de México, México
Received 2024 July 18; revised 2024 September 27; accepted 2024 October 9; published 2024 November 5

Abstract

We analyzed the fractions of barred galaxies in the local Universe using a volume-limited sample of galaxies from the Sloan Digital Sky Survey Data Release 3. We examined 116 field galaxies with redshifts between 0.0207 and 0.030, using r and z-band images. Overall, the bar fraction was 26% in the r-band and 19% in the z-band. For distinct morphological groups, barred spiral galaxies had fractions of 33% in the r-band and 22% in the z-band, while barred lenticular galaxies had 25% in the r-band and 12% in the z-band. We observed that the bar fraction in spiral galaxies increases for stellar masses $\log(M_*/M_\odot) > 10.5$ and for galaxies with red colors $(u-r) > 2.0$. Additionally, most barred galaxies have a bulge-to-total ratio $B/T \leqslant 0.2$. Our results indicate that the bar fraction is more dependent on internal morphology than on the galaxy environment.

Key words: Galaxy: evolution – galaxies: general – galaxies: luminosity function – mass function – Galaxy: disk

1. Introduction

Stellar bars are commonly observed structures in the disks of galaxies, as indicated by several studies (de Vaucouleurs 1963; Knapen et al. 2000; Sheth et al. 2003; Méndez-Abreu et al. 2012; Cervantes Sodi 2017; Erwin 2018). Stellar bars are not only visually impressive, but they also significantly influence the evolution of galaxies by facilitating the transfer of angular momentum between both the baryonic matter and the dark matter within the galaxy (Combes & Sanders 1981; Debattista & Sellwood 2000). Numerous studies have reinforced the idea that the evolution of galaxies is closely connected to the presence and characteristics of stellar bars. Stellar bars are believed to be a crucial internal mechanism influencing the dynamic evolution of disk galaxies. They can alter the central structure and morphology of galaxies by significantly redistributing mass and angular momentum within the disks (Berentzen et al. 2006; Debattista et al. 2006). Moreover, bars are intricately connected to other substructures within galaxies, such as spiral arms, rings, and central dust formations. As bars intensify, spiral arms become more distinct (Buta et al. 2009; Salo et al. 2010; Díaz-García et al. 2019), while rings become smaller (Kim et al. 2012), and dust lanes become more linear (Comerón et al. 2009). According to Athanassoula et al. (2010), the strength of the bar influences the shapes of rings and spiral arms. Bars are commonly characterized by their length and strength. The length and strength of the bar can follow different processes: visually (Martin 1995), through changes in the phase angles of the Fourier modes of the galaxy's light distribution (Quillen et al. 1994; Lee et al. 2022), by variations of the isophotal position angle (PA) (Erwin 2005), identifying the peak in the isophotal ellipticity (Aguerri et al. 2009), by the azimuthally averaged radial profile of the transverse-to-radial force ratio (Lee et al. 2020) or by decomposing the structural components of the galaxy's surface brightness (Gadotti 2011).

The modern understanding of bar growth is based on the angular momentum exchange efficiency between the inner disk (bar in formation) and the outer disk, bulb, halo and, to some degree, with the immediate galactic environment (Athanassoula 2003). This could indicate that there are specific properties of the disks and/or particular processes that intervene in the formation of the galaxy that have a strong impact on the ability to form a bar (Barazza et al. 2008). Therefore, the study of the fraction and the properties of the bars is fundamental to understanding the evolution of disk galaxies (Pérez et al. 2012). Surveys of galaxy redshifts such as the Sloan Digital Sky Survey (SDSS) (Eisenstein et al. 2011) have verified that galaxies are organized in a hierarchical arrangement of filaments and walls, surrounding vast voids in three-dimensional space (Hoyle et al. 2012). Over half of the galaxies (54%) within the nearby Universe ($z \leqslant 0.1$) are found within virialized groups and clusters (Courtois et al. 2013). An additional 20% of galaxies are situated in collapsing regions surrounding groups and clusters (Makarov & Karachentsev 2011). The remaining (26%) of galaxies are categorized as "field" galaxies. In Argudo-Fernández et al. (2015), a more detailed analysis was undertaken to ascertain the proportion of field galaxies observed as either solitary entities, paired isolates, or triplet isolates within the vicinity of the local Universe. Moreover, luminosity functions determined by morphology in the nearby Universe are documented in Nakamura et al. (2004). Their mass function can be approximated using the stellar mass-to-light ratio in the Sloan r-band as provided by Glazebrook et al. (2003). It

has been found that local intermediate mass galaxies are predominantly spirals (70%) and E/S0 (27%) (Hammer et al. 2005). It is proposed that examining intermediate-mass galaxies is essential for comprehending the diversity and evolutionary pathways of galaxies in the nearby Universe. These galaxies serve as a bridge between massive and dwarf galaxies, providing key insights into the processes of galaxy formation and evolution. Moreover, numerous studies have investigated the environmental influence on barred galaxies. Specifically, when considering environmental factors such as proximity to the nearest neighbor, there is a consistent trend observed: the probability of galaxies hosting bars decreases systematically as the distance to the nearest neighbor decreases (Lee et al. 2012; Lin et al. 2014). This observation implies that close encounters may suppress the formation of bars and/or lead to their destruction. On the other hand, if the local environmental density is considered, most of the studies show an independence of barred galaxies with environment (Giordano et al. 2010; Marinova et al. 2012; Sarkar et al. 2021). In cluster environments, the bar fraction in galaxies decreases with cluster mass and proximity to the cluster center, but this relationship disappears depending on the morphological type (Tawfeek et al. 2022). These results may suggest that the formation of bars is influenced by multiple environmental factors and not only by the proximity to the nearest neighbor. These cited studies made a comparative statistical analysis in which their sample included galaxies from clusters as well as field galaxies, and they identified the presence of bars in galaxies. However, it is noteworthy that there are limited studies specifically focused on barred field galaxies. In particular, Durbala et al. (2009) conducted a study on the spiral structure of around 100 isolated galaxies. Their analysis focused on the length and contrast of Fourier bars in relation to galaxy morphology. In another recent study of isolated galaxies by Sánchez-Alarcón et al. (2023), the use of ultra-deep optical images has revealed previously undetected interactions and highlighted the significant influence of internal structures, such as stellar bars, on the morphology of these galaxies. In their study, they build upon such recent research by examining 25 isolated galaxies, identifying new interactions, and emphasizing the crucial role of internal structures in shaping the morphology of these galaxies.

The focus of this study is to ascertain the proportion of barred galaxies within the local Universe, utilizing a representative sample of field galaxies. The rest of the paper is organized as follows. Section 2 details the observational sample. In Section 3, we present the method to detect and characterize the bars in the sample. In Section 4, we present the results and discuss their implications. Finally, in Section 5, we provide a summary and present our overall conclusions.

2. Observational Sample

This study leverages the galaxy sample previously selected by Delgado-Serrano et al. (2010), who utilized the galaxy catalog provided by Fukugita et al. (2007) as the basis for their selection criteria. These galaxies were selected from a sample of 2253 galaxies with Petrosian magnitudes fainter than $r_p = 16$, situated within a 230 deg^2 rectangular area in the equatorial region of the northern celestial hemisphere. Data processing utilized the SDSS Data Release 3 (DR3), with galaxies lacking available spectra being excluded as their study included a morpho-kinematic analysis. They obtained the relative magnitudes from the 2MASS survey (Skrutskie et al. 2006), resulting in a selection of 2113 galaxies. Subsequently, the sample was refined, resulting in 1665 galaxies that met specific criteria, such as an absolute magnitude in the J-band of $M_j < -20.3$, looking for intermediate mass galaxies. Figure 1 shows the distribution of M_j versus redshift in the local SDSS catalog, as reported in Fukugita et al. (2007). It highlights a significant absence of faint galaxies at $z > 0.03$, particularly blue galaxies with magnitudes just below $r_p = 16$. This observation is reinforced by the blue curve, which exhibits a spectral flatness spanning the r-band and J-band, resembling that of a pure starburst near the sample's magnitude threshold. Moreover, all galaxies with $M_j < -20.3$ are encompassed within this sample at $z < 0.03$, totaling 218 galaxies (depicted by red points). Finally, out of these 218 galaxies, only those with spectra containing the [O II]λ3727 emission line were selected, resulting in a final sample of 116 galaxies within the

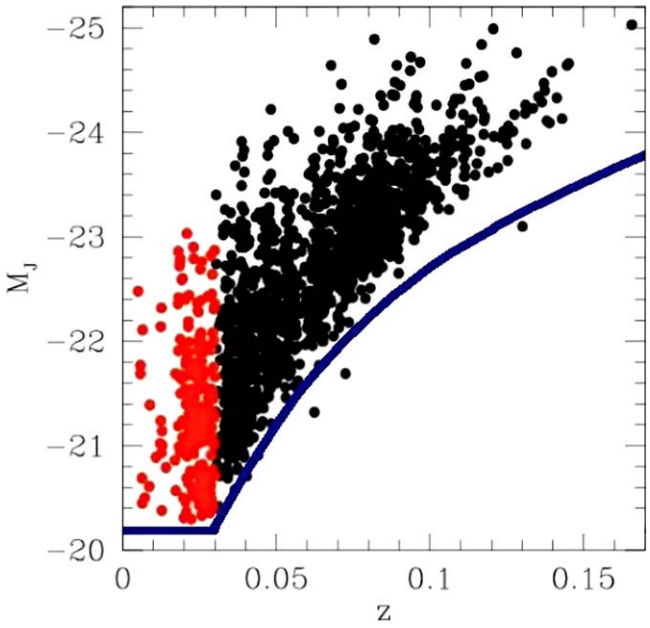

Figure 1. Galaxy sample from Delgado-Serrano et al. (2010) in the M_J vs. z plane. The red points are those included in the selected representative subsample of 218 galaxies. The redshift cut was determined to optimize representativeness in terms of the luminosity function. The curved blue line represents the sample limit assumed to be represented by a blue starburst with $r_p = 16$.

redshift range of $0.0207 \leqslant z \leqslant 0.030$. The validation of the sample of 116 galaxies included comparisons with the local luminosity function as documented by Jones et al. (2006). A Kolmogorov–Smirnov test was performed to evaluate the similarity between this sample and the local luminosity function, showing a high probability of 98% that they exhibit a similar distribution. Therefore, this sample of galaxies is representative of galaxies with $M_j < -20.3$ in the local Universe.

For this study, only data from the r and z-bands were employed. The distribution of morphological types within the sample is as follows: 72% are spirals, 15% lenticular, 3% elliptical, and 10% peculiar. Additional information about this representative sample, including its morphological classification, can be found in Delgado-Serrano et al. (2010). The data set serves as the foundation for our analysis, particularly in detecting bars as outlined in Section 3.

The physical properties for this representative sample, such as stellar mass M^*, are extracted from the MPA/JHU SDSS database (Kauffmann et al. 2003; Brinchmann et al. 2004) and $(u-r)$ color from the Korea Institute for Advanced Study Value-Added Galaxy Catalog (Choi et al. 2010). The bulge-to-total light ratio (B/T) was determined by calculating the ratio of the flux emitted by the bulge to the total flux emitted by the galaxy (Delgado-Serrano et al. 2010), along the major axis using the parameters obtained from the best fit model generated by `Galfit` (Peng et al. 2002). The bulge-to-total (B/T) ratio typically correlates with the Hubble type of galaxy, where early-type galaxies exhibit higher B/T ratios and late-type spirals show lower values.

2.1. Morphological Classification

To ensure reproducibility and reduce subjectivity in morphological classification, Delgado-Serrano et al. (2010) utilized a decision tree adapted from Neichel et al. (2008), tailored to classify elliptical (E), lenticular (S0), and spiral (Sp) galaxies. The decision tree takes into account a range of parameters, including the bulge-to-total (B/T) ratio, half-light radius, `Galfit` parameters, residual and error images, disk-bulge-galaxy profiles, and both two-color maps and three-color images. This approach provides a systematic framework for the classification of galaxies across different samples. To further minimize any remaining subjectivity, three different specialists classified each galaxy independently using the decision tree, later comparing their results. The high level of agreement across classifications demonstrated the effectiveness of this methodology. Notably, the calculations for the `Galfit` model, the B/T ratio, and the morphological classification in our analysis sample were carried out by Delgado-Serrano et al. (2010). Corresponding to the B/T ratio, as described in Neichel et al. (2008), each galaxy is modeled as a combination of a bulge and a disk: the bulge's intensity profile is described using a Sérsic law, while the disk is represented with an exponential function. During the fitting process, all structural parameters, including the Sérsic index, are allowed to vary freely, except for the sky, which was kept fixed at the estimate provided by SExtractor. Additionally, Delgado-Serrano et al. (2010) updated the model used to get B/T by accounting for the alignment between the bulge and disk centers. They observed that, although the bulge+disk fit may appear satisfactory, discrepancies between the centers of the bulge and disk can become apparent in three-color images or residual fit images. Galaxies exhibiting a centroid difference greater than 3 pixels were classified as peculiar (see decision tree for more details in Delgado-Serrano et al. 2010). In addition to the above, for the present study, we further checked some parameters as follows: (1) We compared values of B/T ratio obtained for each galaxy of the sample by Delgado-Serrano et al. (2010) with those corresponding B/T values in the catalog from Simard et al. (2011), finding a good agreement. (2) We verified visually, galaxy by galaxy, in the Legacy Survey to verify the existence or not of spiral structures or any other visual discrepancy with classification. We did not find any discrepancy. (3) We inspected the residual images of the simulations performed with IRAF for the calculation of ellipticity and PA (see Section 3), looking for any features inconsistent with the morphological classification reported, but we did not find any inconsistencies. We focused on three main galaxy types:

1. *Elliptical (E) galaxies*. These galaxies are defined by a B/T ratio between 0.8 and 1.0. They exhibit smooth, featureless light distributions with no visible disk structure, representing the classic elliptical morphology.
2. *Lenticular (S0) galaxies*. Characterized by a B/T ratio between 0.5 and 0.8, these galaxies lack spiral arms. The bulge is redder than the disk, and there is a close alignment between the centers of the bulge and disk, which are highly symmetrical.
3. *Spiral (Sp) galaxies*. These galaxies have a distinct disk structure with spiral arms and a B/T ratio below 0.5. The bulge is redder than the disk, and there is a strong alignment between the bulge and disk centers, contributing to a highly symmetric appearance.

This classification scheme allows for a clear distinction between the main structures of galaxies, especially highlighting the separation between spiral and lenticular galaxies in contrast to ellipticals.

2.2. Field Galaxies

Studying bars in field galaxies is crucial for comprehensively understanding their formation and evolution across various galactic environments. Although research has predominantly focused on cluster and combined environments, exploring the characteristics of bars in field galaxies may provide a unique perspective. These comparisons allow for discerning significant

Table 1
Diverse Criteria for Bar Detection Using Ellipse Fitting Method

Study	ΔPA_{bar}	ε_{bar}	f_{bar}	Wavelength	Redshift
Wozniak et al. (1995)	const	⋯	⋯	*B*, *V*, *R*, *I*	∼0.01
Laine et al. (2002)	±10°	$\varepsilon_{max} \geqslant 0.45$	55	*NIR*	∼0.01
Jogee et al. (2004)	±20°	$\varepsilon_{max} \geqslant 0.4$	33	*Optics*	0.25–0.7
Menéndez-Delmestre et al. (2007)	const	$\varepsilon_{max} \geqslant 0.2$	59	$J + H + K$	∼0.01
Marinova & Jogee (2007)	±5°	⩾0.25	44 ± 7	*Optics*	∼0.01
			60 ± 7	*NIR*	∼0.01
Barazza et al. (2008)	±5°	$\varepsilon_{max} \geqslant 0.25$	48	*r*-band	0.01–0.03
Sheth et al. (2008)	const	⩾0.2	65	*NIR*	∼0.2
Aguerri et al. (2009)	±10°	⋯	45	*r*-band	0.01–0.04
Marinova et al. (2009)	±10°	$\varepsilon_{max} \geqslant 0.25$	∼30	*Optics*	∼0.165
Marinova et al. (2012)	±10°	$\varepsilon_{max} \geqslant 0.25$	50 ± 11	*NIR*	∼0.02
Consolandi et al. (2016)	±20°	⋯	36	*Optics*	∼0.01
Lee et al. (2019)	±5°	$\varepsilon_{max} \geqslant 0.25$	48	*g*-band	∼0.01
Yoon et al. (2019)	±5°	$\varepsilon_{max} \geqslant 0.25$	27 and 42	*r*-band	0.01–0.06
Tawfeek et al. (2022)	±20°	⋯	∼26	*V*-band	0.04–0.07
Sánchez-García et al. (2023)	±5°	⋯	29	*r*-band	0.04–0.07

Note. Based on the original table from Lee et al. (2019).

differences in the frequency, morphology, and effects of bars in different environments, thereby revealing their role in galactic evolution. To ensure that our galaxy selection includes only field galaxies, a comparison was made with the galaxy group catalog by Lim et al. (2017). This catalog, which utilizes a halo-based group finder applied to large redshift surveys like the SDSS and 2MASS Redshift Survey (2MRS), identifies galaxy groups and their properties. The comparison assessed whether the selected galaxies are central galaxies within these groups and determined the number of group members associated with each galaxy. We observed that 60% of spiral galaxies and 40% of lenticular galaxies are isolated. The remaining galaxies in our sample exhibit a comparatively small number of group members, and it was determined that they are the central galaxies within their respective groups.

Another important consideration involved determining the distance to the closest neighbor galaxy, considering galaxies not fainter than the target galaxy by more than 0.5 mag in the *r*-band and a radial velocity difference with that of the target galaxy $\Delta v \leqslant 800\,\mathrm{km\,s^{-1}}$. The result indicated that these galaxies did not show any interaction with other galaxies, hence, confirming that our representative sample is composed of relatively isolated field galaxies.

3. Bar Classification Methodology

Bars can be identified using various methods such as visual inspection, multicomponent decomposition, Fourier analysis, and ellipse isophotal fitting. Visual inspection is widely adopted and highly effective in detecting bars, boasting a high success rate (Sheth et al. 2008; Buta et al. 2010; Lin et al. 2014). The isophotal fitting technique involves characterizing bars and disks in galaxies through the fit of elliptical isophotes (Sheth et al. 2003; Zheng et al. 2005; Marinova & Jogee 2007; Consolandi et al. 2016; Chacón & Delgado-Serrano 2019; Lee et al. 2019; Sánchez-García et al. 2023). We detect the presence of a bar within a galaxy disk by analyzing the characteristic changes in ellipticity (ε) and PA profiles traced by the galaxy isophotes. This analysis is performed using the `IRAF` task `ellipse`. In summary, this methodology entails fitting ellipses to the tracer images as described by Jedrzejewski (1987), followed by applying quantitative criteria to identify bars. The `ellipse` task necessitates initial values for isophotal analysis, for which we utilize the `SExtractor` software (Bertin & Arnouts 1996). The criteria for identifying bars using the ellipse fitting has undergone some variations over time. Lee et al. (2019) provide a list of these criteria and the results of the bar fraction found in those studies, see Table 1. The main difference between the studies mentioned in Table 1 and our own lies in the sample sizes. While those studies utilized large data sets, our sample was selected using specific representative criteria, as explained earlier. This approach ensures that the galaxies chosen reflect a broad spectrum of morphological characteristics, such as the precise distinction between elliptical, lenticular, and spiral galaxies. Unlike larger studies that may depend on bulk classifications or automated methods, our methodology emphasizes accuracy and reduces the likelihood of misclassification, offering deeper insights into the structural and evolutionary properties of these galaxies.

For our representative galaxy sample, we employed ellipse fitting to categorize galaxies as either "unbarred" (Figure 2) or "barred" (Figure 3), based on specific quantitative criteria. A galaxy is categorized as barred if the radial variation of ellipticity and PA conforms to the expected behavior

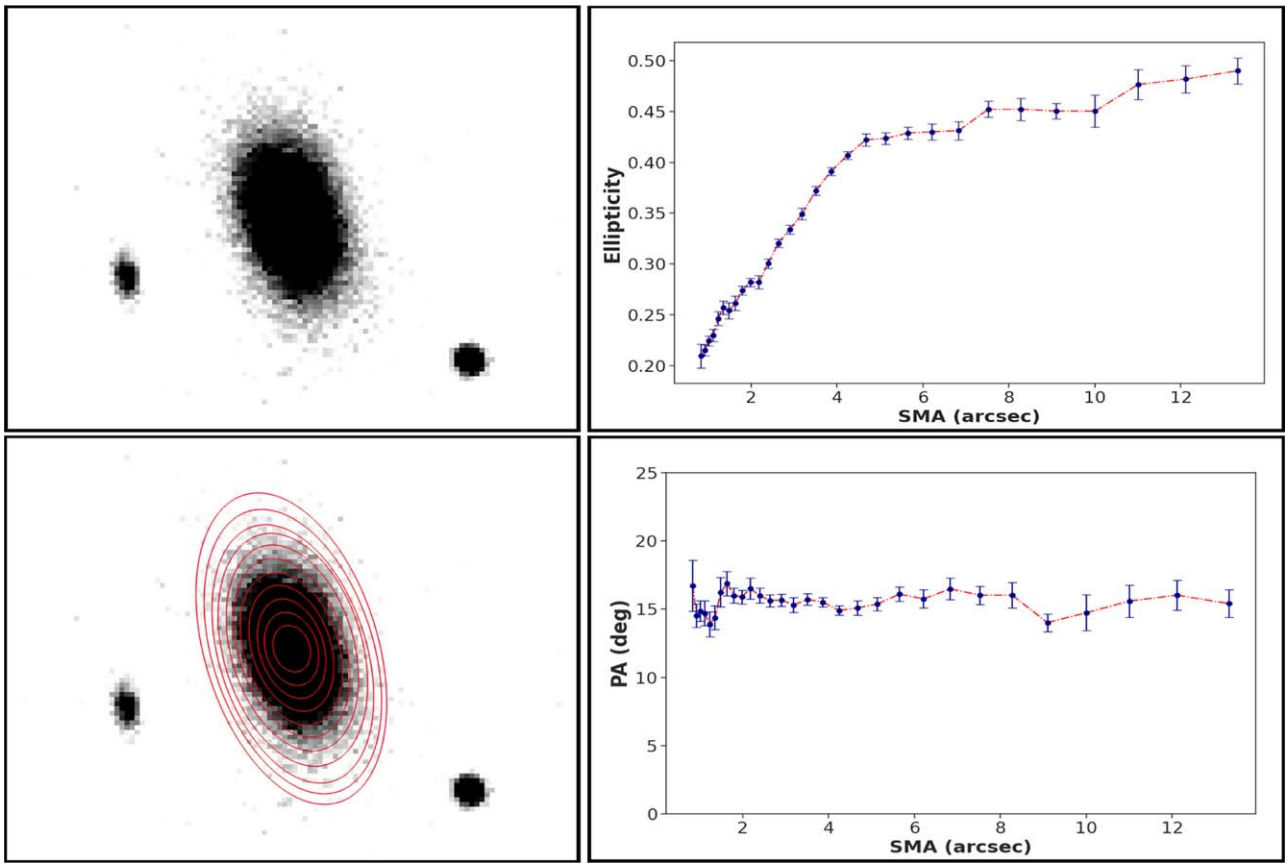

Figure 2. Example of an unbarred galaxy from our sample. From left to right: the top row shows the original *r*-band image, and below it, the isophotal analysis. On the right, the top row displays the isophotal ellipticity radial profile as a function of the semimajor axis (SMA), and below it, the PA radial profile of the isophotes as a function of the SMA.

determined by the dominant orbits within a barred potential (Marinova & Jogee 2007). Specifically, a galaxy is classified as barred if the following conditions are met: (a) The ellipticity (ε) increases steadily to a global maximum, $\varepsilon_{\rm bar} \geqslant 0.25$, while the $\Delta {\rm PA}_{\rm bar}$ value remains relatively constant (within $\pm 10^{\circ}$). (b) At the transition from the bar to the disk region, there should be a decrease in ellipticity ε of at least $\Delta\varepsilon \geqslant 0.1$, and a change in position angle ($\Delta {\rm PA} \geqslant 10^{\circ}$) of more than 10°. (c) In SDSS images, the point-spread function (PSF) has a full width at half maximum (FWHM) of approximately $\sim 1\farcs4$, with a pixel scale of $0\farcs396$ pixel^{-1} (Jackson et al. 2008; Consolandi et al. 2016). We use this mean PSF for the SDSS images. During the initial iterations of the isophotes (lines of equal brightness), significant oscillations often appear due to initial adjustments. To reduce dispersion and improve accuracy, we use the criterion of removing the first 2 pixels from the graphs obtained with the `ellipse` tool.

4. Results and Discussion

The bar fraction is defined as $f_{\rm bar} = \frac{g_{\rm bar}}{N}$, where $g_{\rm bar}$ represents the number of barred galaxies and N the total number of galaxies. To mitigate inclination bias, the sample of spiral and lenticular galaxies is constrained to systems with *r*- and *z*-band isophotal axis ratio $b/a > 0.6$ (Lee et al. 2012). This restriction minimizes selection bias arising from galaxy inclination, where a and b represent the semimajor and semiminor axes, respectively. This ratio was calculated from images using `SExtractor`.

The uncertainties-throughout this work-represent 1σ confidence intervals determined by the bootstrap resampling method, conducted through 1000 iterations to ensure the robustness and reliability in our results.

Our study focused on determining the prevalence of barred galaxies within our representative sample of field galaxies. Initially, we calculated the bar fraction percentage for the entire sample, revealing values of $26\% \pm 15\%$ using *r*-band and $19\% \pm 12\%$ using *z*-band. The disparity in bar fraction between the *r* and *z*-bands can be attributed to the differing sensitivity of these filters, which is influenced by their respective transmission curves. The *r*-band filter, being shorter in wavelength and corresponding to bluer light, is better suited to capture features such as the surface brightness of bars and their contrast with the

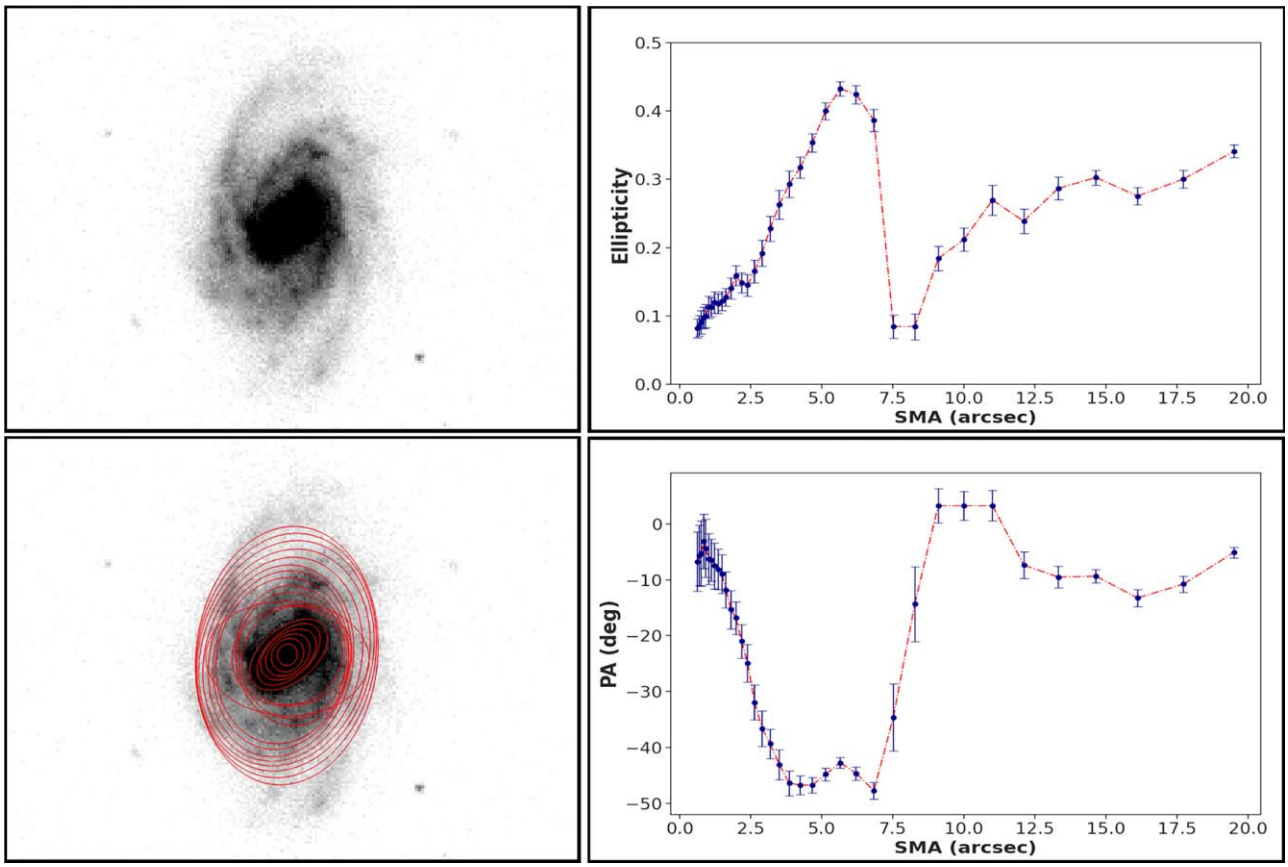

Figure 3. Example of a barred galaxy from our sample. From left to right: the top row shows the original *r*-band image, and below it, the isophotal analysis. On the right, the top row displays the isophotal ellipticity radial profile as a function of the SMA, and below it, the PA radial profile of the isophotes as a function of the SMA.

galactic disk. Consequently, it is more adept at detecting barred structures, particularly those prominent in bluer wavelengths where younger stars are prevalent. In contrast, the *z*-band filter, with its longer wavelength, may have reduced sensitivity to weaker barred structures, especially if they are primarily visible in bluer wavelengths. Significantly, to enhance sensitivity in the *z*-band for detecting weaker barred structures, longer exposure times in the images would be necessary. This difference in sensitivity, shaped by the transmission curves of the filters, explains the observed disparity in the fraction of barred galaxies between the *r* and *z* bands. Notably, given the higher sensitivity of the *r*-band filter to detect barred structures, it may be more feasible to focus on this filter for this investigation.

Figure 4 shows the bar fraction for two morphological groups of galaxies in the *r*-band. It illustrates that $33\% \pm 13\%$ of spiral galaxies are barred and $25\% \pm 16\%$ lenticular galaxies are barred. These values are, on one hand, in good agreement with studies that detect bars using the ellipse fitting method (Table 1) using much larger samples and including both cluster and field galaxies. On the other hand, however, our result differs from those in Buta et al. (2019) and Verley et al. (2007), who studied samples of isolated local galaxies. Verley et al. (2007) using a sample of 45 isolated spiral galaxies from the Analysis of the Interstellar Medium of Isolated Galaxies (AMIGA) catalog, within a range of heliocentric recession velocities from 1500 to 5000 $\mathrm{km\,s^{-1}}$ with SMA $\geqslant 1'$ and $i \leqslant 50$, found that 60% of the studied galaxies had bars. Buta et al. (2019) using 719 Catalog of Isolated Galaxies with redshift range of $0.005 \leqslant z \leqslant 0.080$; and $i \leqslant 60$, found a bar fraction of ≈50% (16% strongly barred). Both Verley et al. (2007) and Buta et al. (2019) used a different morphological classification method, a different representative analysis and different bar detection method than in our study.

Looking at our results, in the *z*-band, we found that $22\% \pm 12\%$ of spiral and $12\% \pm 9\%$ of lenticular galaxies are barred. Significantly, we observed that more exposure time is needed in the images to allow the task `ellipse` to complete the iteration over the different structures in the galaxies. In the results obtained from the entire representative sample of field galaxies, we did not detect bars in the following morphological groups: elliptical galaxies and peculiar galaxies.

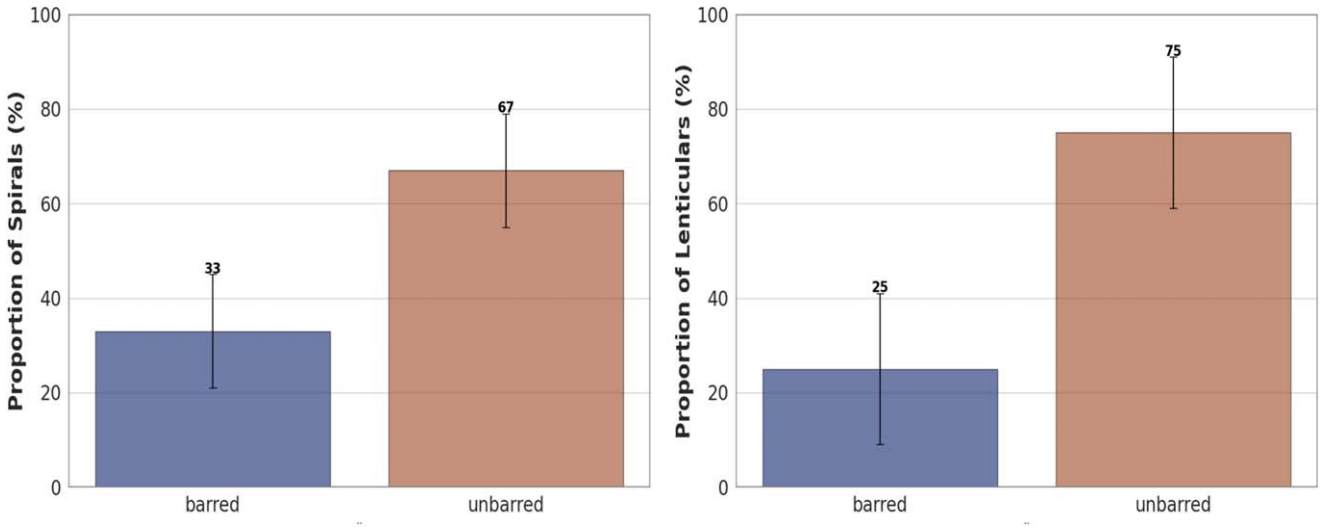

Figure 4. Fraction of barred and unbarred galaxies for the spirals (left panel) and lenticular (right panel) galaxies of the galaxy sample.

Figure 5(a) illustrates the dependence of $f_{\rm bar}$ on stellar mass (Méndez-Abreu et al. 2010) for the spiral galaxies in our sample, and there is an increase in the bar fraction with increasing stellar mass log $(M_*/M_\odot) > 10.50$. In Cervantes Sodi et al. (2015), addressing mixed environments in the r-band in SDSS Data Release 7 (DR7), it was noted that for high-mass galaxies with log $(M_*/M_\odot) > 10.50$, the bar fraction of satellite galaxies surpasses that of central galaxies. This trend is particularly pronounced for strong bars. This pattern is reminiscent of the bar fraction trend reported in Díaz-García et al. (2016). They used 3.6 μm imaging from the Spitzer Survey of Stellar Structure in Galaxies (S^{4}G) to study the properties and fraction of bars at $z = 0$ across a wide range of galaxy masses ($M_* \sim 10^8$–$10^{11} M_\odot$) and Hubble types ($-3 \leqslant T \leqslant 10$). They found a dependence between $f_{\rm bar}$ and the total stellar mass but did not observe a clear trend from the visual classification of bars for galaxies with stellar masses log $(M_*/M_\odot) \geqslant 9$. Nevertheless, methods based on Fourier decomposition (Buta et al. 2015) and ellipse fitting, applied to detect bars in S^{4}G, reveal that $f_{\rm bar}$ increases with stellar mass up to log $(M_*/M_\odot) \sim 9.5$–10, where it reaches a constant level of ∼50% in the range of log $(M_*/M_\odot) \sim 10$–11, with a distinct peak (∼60%) at log $(M_*/M_\odot) \sim 10.5$. Notably, we observed a similar relationship between the fraction of bars and stellar mass in our representative field galaxy sample, with a secondary peak in $f_{\rm bar}$ observed at log $(M_*/M_\odot) \sim 10.6$.

In Figure 5(b), we illustrate the dependence of $f_{\rm bar}$ on $(u - r)$. Our sample shows a significant fraction of host galaxies with red colors $(u - r) > 2.0$. To avoid the problem of internal absorption in edge-on galaxies (Unterborn & Ryden 2008; Cho & Park 2009), we limit the sample to late-type galaxies having seeing-corrected isophotal axis ratios $b/a > 0.6$, where the identification of bars is also more reliable.

In Masters et al. (2011), using a large sample comprising both cluster and field galaxies, strong trends were reported between bar fraction and galaxy optical color. Specifically, redder galaxies were found to be much more likely to exhibit bars. This finding indicates that red spiral galaxies undergoing passive evolution are more inclined to possess a strong bar compared to blue spirals that show ongoing star formation activity. These patterns are in line with the conclusions drawn by Hoyle et al. (2011), indicating that longer bars are more prevalent in late-type galaxies, while shorter bars are typically found in bluer late-type galaxies. Moreover, the proportion of late-type galaxies exhibiting a prominent bar increases notably as the $(u - r)$ color index rises: it remains below 20% for galaxies with $(u - r) = 2.0$, but increases to 45% around $(u - r) \sim 2.8$, before declining toward the redder end of the spectrum (Lee et al. 2012). This observation indicates that red spiral galaxies undergoing passive evolution are more prone to host strong bars compared to blue spirals engaged in ongoing star formation. Conversely, Tawfeek et al. (2022) present contradictory findings. They observe a significant negative correlation between the frequency of bars $f_{\rm bar}$ and the $(B - V)$ color index, suggesting a notable reduction in bar occurrence as $(B - V)$ values increase. Their study utilized a sample of clusters derived from V-band images of 32 clusters selected from the OmegaWINGS photometric catalog (Gullieuszik et al. 2015). Their sample notably comprises cluster galaxies, an environment recognized for inducing significant transformations in both stellar populations and morphology. This discrepancy with our trend arises from an environmental effect that is not present in field galaxies. While the group/cluster environment does not directly impact the bar fraction, its influence is mediated through internal morphology.

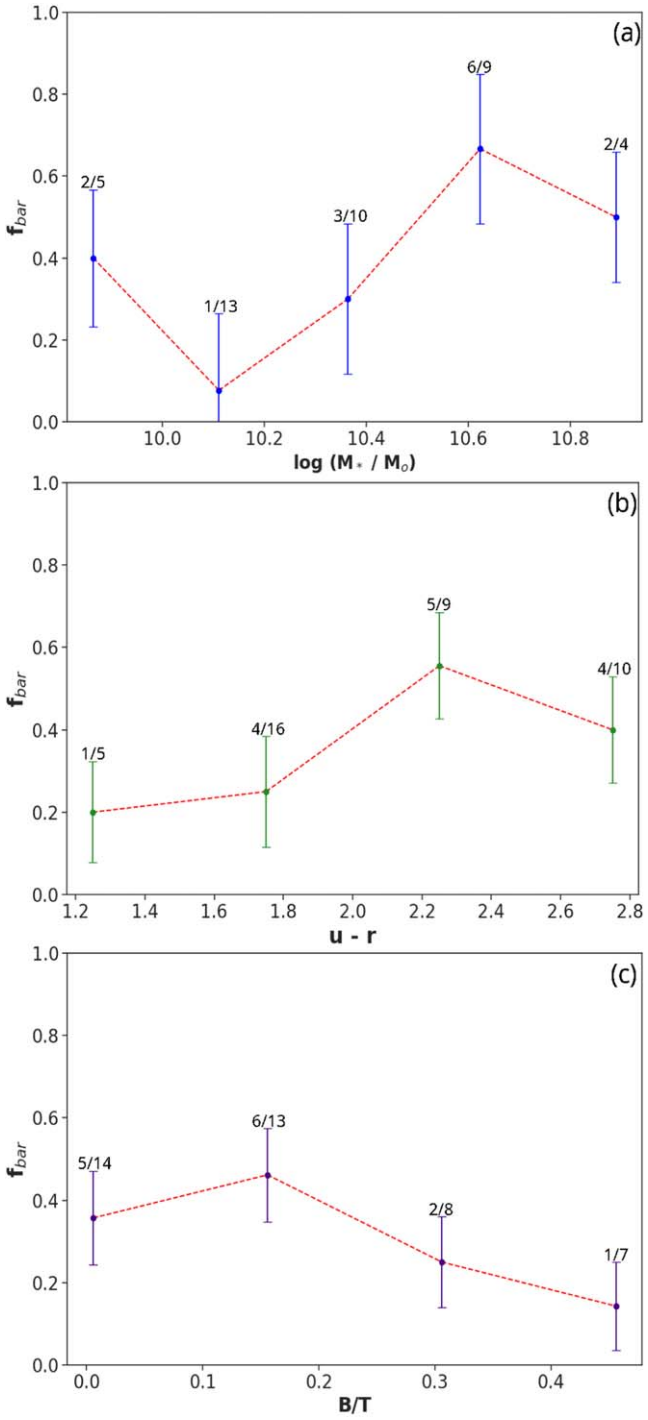

Figure 5. Bar fraction of spiral galaxies $f_{\rm bar}$ as a function of (a) stellar mass, (b) $(u-r)$ color, and (c) bulge-to-total B/T ratio. Each panel includes the bar fraction in each bin.

Figure 5(c) illustrates the dependence of $f_{\rm bar}$ on B/T for spiral galaxies in our sample, where the majority of barred galaxies exhibit $B/T \leqslant 0.2$, consistent with findings from previous studies (Aguerri et al. 2009; Yoon et al. 2019). Previous numerical simulations also support the conclusion that the formation or maintenance of bars is inhibited in galaxies with high B/T or high central mass concentrations (Shen & Sellwood 2004; Athanassoula et al. 2005; Bournaud et al. 2005). According to Weinzirl et al. (2009), galaxies with a low bulge-to-disk ratio B/T tend to have bars. Specifically, around 65% of spirals with low-mass concentration bulges ($n \leqslant 2$) host bars, while systems with $B/T \leqslant 0.2$ have a high probability of having bars (approximately 68%). Other studies of late-type spiral galaxies indicate that bulge-dominated spirals have a smaller fraction of barred galaxies compared to disk-dominated ones (Barazza et al. 2008). Moreover, recent simulation studies of galaxies have determined that the strength of the bar is influenced independently by two factors: gas fraction and bulge fraction. Galaxies devoid of gas and bulges tend to develop strong bars, while those rich in gas and with substantial bulges tend to show minimal bar formation. In essence, the presence of gas and bulges acts to suppress the formation of bars in galaxies (Machado et al. 2024).

Our results, in agreement with previous studies working with samples of mixed environments, highlight the importance of the internal structural parameters of galaxies in the presence of bars in the local Universe. Our findings confirm that while the fraction of galaxies with bars does not depend solely on their environment, it is also influenced by internal characteristics such as stellar mass, color and bulge-to-disk ratio. This emphasizes the complexity of the factors influencing bar formation and the need to consider both internal processes and external influences in galaxy evolution.

5. Summary and Conclusions

The main objective of this study was to determine the proportion of barred field galaxies in the local Universe, utilizing a representative sample of field galaxies. We utilized r-band and z-band images from SDSS DR3 to investigate the existence of bars in local field galaxies. A representative sample of 116 galaxies has been analyzed in both bands. We applied the ellipse fitting technique as a method for bar detection. Here, we summarize and discuss our main results:

(i) We determined the percentage of barred galaxies in our entire sample, finding $26\% \pm 15\%$ for the r-band and $19\% \pm 12\%$ for the z-band. The disparity in bar fraction between the r and z-bands is due to differing filter sensitivities. The r-band, with its shorter wavelength, better detects barred structures, especially in bluer wavelengths, while the z-band has reduced sensitivity to galaxy structures. Upon further categorization of the sample based on morphology, we observed that barred spiral galaxies accounted for $f_{\rm bar} = 33\% \pm 13\%$ in the r-band, and barred lenticular galaxies for $f_{\rm bar} = 25\% \pm 16\%$. In the z-band, the percentages were $f_{\rm bar} = 22\% \pm 12\%$ for spiral galaxies and $f_{\rm bar} = 12\% \pm 9\%$ for lenticular galaxies. These results,

derived from our representative sample of field galaxies, closely align with previous findings from studies with much larger data sets encompassing galaxies from mixed environments.

(ii) The bar fraction tends to be higher at approximately log $(M_*/M_\odot) \sim 10.6$ stellar masses. This suggests that more massive galaxies are more likely to host bars in their structure. One possible explanation is that more massive galaxies show a greater tendency to lie on the red sequence, indicating lower star formation activity, which favors the formation and persistence of bars. Additionally, more massive galaxies have more self-gravitating disks, where bar instabilities can arise and develop. This can occur even in isolated galaxies, without the need for external triggers such as neighboring galaxies or denser environments.

(iii) The dependence of $f_{\rm bar}$ as a function of $(u-r)$ color highlights a significant increase as the color shifts toward redder hues. Red spiral galaxies undergoing passive evolution are more likely to exhibit a strong bar compared to blue spirals that are actively undergoing star formation.

(iv) Our representative sample indicates that spiral galaxies with $B/T \leqslant 0.2$ are more likely to harbor bars in their structure. Given that massive bulges can form through mergers, this result might indicate that a quieter assembly history could favor the formation of bars or bars are formed in late stages in the merger process. Our result also confirms that a massive central concentration of mass, supported by velocity dispersion, stabilizes galaxies against bar formation.

(v) In our sample of field galaxies, bars were not found in elliptical or peculiar galaxies, where bars might be formed exclusively through external perturbations.

In summary, this investigation highlights the importance of examining field galaxies through representative samples. This finding, consistent with previous studies, affirms that the bar fraction is not solely influenced by galaxy environment but is strongly dependent on structural parameters and the overall morphology of the galaxies. Factors such as disk structure and stellar mass distribution are crucial in bar formation, underscoring the significance of intrinsic characteristics in the morphological evolution of galaxies. Although the sample size is small, a rigorous selection process based on mass and morphological classification was applied to ensure the quality and relevance of the data. Understanding the role of bars in field galaxies is essential for gaining deeper insights into their formation and evolution across various galactic environments.

Acknowledgments

We gratefully acknowledge financial support from the Secretaría Nacional de Ciencia, Tecnología e Innovación (SENACYT), through the Departamento de Fortalecimiento a los Posgrados Nacionales and the coordination of the program "MOVILIDAD DE INVESTIGACIÓN," for the project "Formación de capacidades investigativas en la línea de Astronomía Extragaláctica 005-2023." I also thank the support of the Programa de Apoyo a Proyectos de Investigación e Innovación Tecnológica (PAPIIT) IN108323 from the Dirección General de Asuntos del Personal Académico (DGAPA-UNAM). The authors thank the anonymous referee for useful comments that helped to improve the quality of the paper and clarify our results. This study is built upon data obtained from the Sloan Digital Sky Survey (SDSS). Funding for the SDSS and SDSS-II has been provided by the Alfred P. Sloan Foundation and Participating Institutions, the National Science Foundation, the U.S. Department of Energy, the National Aeronautics and Space Administration, the Japanese Monbukagakusho, the Max Planck Society, and the Higher Education Funding Council for England. The SDSS website is www.sdss.org. The SDSS is managed by the Astrophysical Research Consortium for the Participating Institutions. The participating institutions are the American Museum of Natural History, Astrophysical Institute Potsdam, University of Basel, University of Cambridge, Case Western Reserve University, University of Chicago, Drexel University, Fermilab, the Institute for Advanced Study, the Japan Participation Group, Johns Hopkins University, the Joint Institute for Nuclear Astrophysics, the Kavli Institute for Particle Astrophysics and Cosmology, the Korean Scientist Group, the Chinese Academy of Sciences (LAMOST), Los Alamos National Laboratory, the Max-Planck-Institute for Astronomy (MPIA), the Max-Planck-Institute for Astrophysics (MPA), New Mexico State University, Ohio State University, University of Pittsburgh, University of Portsmouth, Princeton University, the United States Naval Observatory, and the University of Washington.

References

Aguerri, J. A. L., Méndez-Abreu, J., & Corsini, E. M. 2009, A&A, 495, 491
Argudo-Fernández, M., Verley, S., Bergond, G., et al. 2015, A&A, 578, A110
Athanassoula, E. 2003, MNRAS, 341, 1179
Athanassoula, E., Lambert, J. C., & Dehnen, W. 2005, MNRAS, 363, 496
Athanassoula, E., Romero-Gómez, M., Bosma, A., & Masdemont, J. J. 2010, MNRAS, 407, 1433
Barazza, F. D., Jogee, S., & Marinova, I. 2008, ApJ, 675, 1194
Berentzen, I., Shlosman, I., & Jogee, S. 2006, ApJ, 637, 582
Bertin, E., & Arnouts, S. 1996, A&AS, 117, 393
Bournaud, F., Combes, F., & Semelin, B. 2005, MNRAS, 364, L18
Brinchmann, J., Charlot, S., White, S. D. M., et al. 2004, MNRAS, 351, 1151
Buta, R. J., Knapen, J. H., Elmegreen, B. G., et al. 2009, AJ, 137, 4487
Buta, R. J., Sheth, K., Athanassoula, E., et al. 2015, ApJS, 217, 32
Buta, R. J., Sheth, K., Regan, M., et al. 2010, ApJS, 190, 147
Buta, R. J., Verdes-Montenegro, L., Damas-Segovia, A., et al. 2019, MNRAS, 488, 2175
Cervantes Sodi, B. 2017, ApJ, 835, 80
Cervantes Sodi, B., Li, C., & Park, C. 2015, ApJ, 807, 111
Chacón, M. A., & Delgado-Serrano, R. 2019, in 2019 7th Int. Engineering, Sciences and Technology Conference (IESTEC) (Piscataway, NJ: IEEE), 92
Cho, J., & Park, C. 2009, ApJ, 693, 1045

Choi, Y.-Y., Han, D.-H., & Kim, S. 2010, JKAS, 43, 191
Combes, F., & Sanders, R. H. 1981, A&A, 96, 164
Comerón, S., Martínez-Valpuesta, I., Knapen, J. H., & Beckman, J. E. 2009, ApJL, 706, L256
Consolandi, G., Gavazzi, G., Fumagalli, M., Dotti, M., & Fossati, M. 2016, A&A, 591, A38
Courtois, H. M., Pomarède, D., Tully, R. B., Hoffman, Y., & Courtois, D. 2013, AJ, 146, 69
de Vaucouleurs, G. 1963, ApJS, 8, 31
Debattista, V. P., Mayer, L., Carollo, C. M., et al. 2006, ApJ, 645, 209
Debattista, V. P., & Sellwood, J. A. 2000, ApJ, 543, 704
Delgado-Serrano, R., Hammer, F., Yang, Y. B., et al. 2010, A&A, 509, A78
Díaz-García, S., Salo, H., Knapen, J. H., & Herrera-Endoqui, M. 2019, A&A, 631, A94
Díaz-García, S., Salo, H., Laurikainen, E., & Herrera-Endoqui, M. 2016, A&A, 587, A160
Durbala, A., Buta, R., Sulentic, J. W., & Verdes-Montenegro, L. 2009, MNRAS, 397, 1756
Eisenstein, D. J., Weinberg, D. H., Agol, E., et al. 2011, AJ, 142, 72
Erwin, P. 2005, MNRAS, 364, 283
Erwin, P. 2018, MNRAS, 474, 5372
Fukugita, M., Nakamura, O., Okamura, S., et al. 2007, AJ, 134, 579
Gadotti, D. A. 2011, MNRAS, 415, 3308
Giordano, L., Tran, K.-V. H., Moore, B., & Saintonge, A. 2010, arXiv:1002.3167
Glazebrook, K., Baldry, I. K., Blanton, M. R., et al. 2003, ApJ, 587, 55
Gullieuszik, M., Poggianti, B., Fasano, G., et al. 2015, A&A, 581, A41
Hammer, F., Flores, H., Elbaz, D., et al. 2005, A&A, 430, 115
Hoyle, B., Masters, K. L., Nichol, R. C., et al. 2011, MNRAS, 415, 3627
Hoyle, F., Vogeley, M. S., & Pan, D. 2012, MNRAS, 426, 3041
Jackson, N., Ofek, E. O., & Oguri, M. 2008, MNRAS, 387, 741
Jedrzejewski, R. I. 1987, MNRAS, 226, 747
Jogee, S., Barazza, F. D., Rix, H.-W., et al. 2004, ApJL, 615, L105
Jones, D. H., Peterson, B. A., Colless, M., & Saunders, W. 2006, MNRAS, 369, 25
Kauffmann, G., Heckman, T. M., White, S. D. M., et al. 2003, MNRAS, 341, 33
Kim, W.-T., Seo, W.-Y., & Kim, Y. 2012, ApJ, 758, 14
Knapen, J. H., Shlosman, I., & Peletier, R. F. 2000, ApJ, 529, 93
Laine, S., Shlosman, I., Knapen, J. H., & Peletier, R. F. 2002, ApJ, 567, 97
Lee, G.-H., Park, C., Lee, M. G., & Choi, Y.-Y. 2012, ApJ, 745, 125
Lee, Y. H., Ann, H. B., & Park, M.-G. 2019, ApJ, 872, 97
Lee, Y. H., Park, M.-G., Ann, H. B., Kim, T., & Seo, W.-Y. 2020, ApJ, 899, 84
Lee, Y. H., Park, M.-G., Hwang, H. S., et al. 2022, ApJ, 926, 58
Lim, S. H., Mo, H. J., Lu, Y., Wang, H., & Yang, X. 2017, MNRAS, 470, 2982
Lin, Y., Cervantes Sodi, B., Li, C., Wang, L., & Wang, E. 2014, ApJ, 796, 98
Machado, R. E. G., Sakamoto, K. R., Wille, A., & Gonçalves, G. F. 2024, Univ, 10, 223
Makarov, D., & Karachentsev, I. 2011, MNRAS, 412, 2498
Marinova, I., & Jogee, S. 2007, ApJ, 659, 1176
Marinova, I., Jogee, S., Heiderman, A., et al. 2009, ApJ, 698, 1639
Marinova, I., Jogee, S., Weinzirl, T., et al. 2012, ApJ, 746, 136
Martin, P. 1995, AJ, 109, 2428
Masters, K. L., Nichol, R. C., Hoyle, B., et al. 2011, MNRAS, 411, 2026
Méndez-Abreu, J., Sánchez-Janssen, R., & Aguerri, J. A. L. 2010, ApJL, 711, L61
Méndez-Abreu, J., Sánchez-Janssen, R., Aguerri, J. A. L., Corsini, E. M., & Zarattini, S. 2012, ApJL, 761, L6
Menéndez-Delmestre, K., Sheth, K., Schinnerer, E., Jarrett, T. H., & Scoville, N. Z. 2007, ApJ, 657, 790
Nakamura, O., Fukugita, M., Brinkmann, J., & Schneider, D. P. 2004, AJ, 127, 2511
Neichel, B., Hammer, F., Puech, M., et al. 2008, A&A, 484, 159
Peng, C. Y., Ho, L. C., Impey, C. D., & Rix, H.-W. 2002, AJ, 124, 266
Pérez, I., Aguerri, J. A. L., & Méndez-Abreu, J. 2012, A&A, 540, A103
Quillen, A. C., Frogel, J. A., & Gonzalez, R. A. 1994, ApJ, 437, 162
Salo, H., Laurikainen, E., Buta, R., & Knapen, J. H. 2010, ApJL, 715, L56
Sánchez-Alarcón, P. M., Román, J., Knapen, J. H., et al. 2023, A&A, 677, A117
Sánchez-García, O., Cervantes Sodi, B., Fritz, J., et al. 2023, ApJ, 945, 99
Sarkar, S., Pandey, B., & Bhattacharjee, S. 2021, MNRAS, 501, 994
Shen, J., & Sellwood, J. A. 2004, ApJ, 604, 614
Sheth, K., Elmegreen, D. M., Elmegreen, B. G., et al. 2008, ApJ, 675, 1141
Sheth, K., Regan, M. W., Scoville, N. Z., & Strubbe, L. E. 2003, ApJL, 592, L13
Simard, L., Mendel, J. T., Patton, D. R., Ellison, S. L., & McConnachie, A. W. 2011, ApJS, 196, 11
Skrutskie, M. F., Cutri, R. M., Stiening, R., et al. 2006, AJ, 131, 1163
Tawfeek, A. A., Cervantes Sodi, B., Fritz, J., et al. 2022, ApJ, 940, 1
Unterborn, C. T., & Ryden, B. S. 2008, ApJ, 687, 976
Verley, S., Combes, F., Verdes-Montenegro, L., Bergond, G., & Leon, S. 2007, A&A, 474, 43
Weinzirl, T., Jogee, S., Khochfar, S., Burkert, A., & Kormendy, J. 2009, ApJ, 696, 411
Wozniak, H., Friedli, D., Martinet, L., Martin, P., & Bratschi, P. 1995, A&AS, 111, 115
Yoon, Y., Im, M., Lee, G.-H., Lee, S.-K., & Lim, G. 2019, NatAs, 3, 844
Zheng, X. Z., Hammer, F., Flores, H., Assémat, F., & Rawat, A. 2005, A&A, 435, 507